Gargallo Bellés, S.; Martín Monerris, M.; Oliver Rajadel, N.; Hernández Crespo, C. (2016). Sedimentation and resuspension modelling in free water surface constructed wetlands. Ecological Engineering. 98:318-329. doi:10.1016/j.ecoleng.2016.09.014

SEDIMENTATION AND RESUSPENSION MODELLING IN FREE WATER SURFACE CONSTRUCTED WETLANDS

S. Gargallo[1]*, M. Martín[1], N. Oliver[1], C. Hernández-Crespo[1]

[1]Research Institute of Water and Environmental Engineering,

Universitat Politècnica de València, Cno. de Vera s/n, Valencia, Spain

sagarbel@upv.es

Abstract

Eutrophication is a widespread problem that is being tackled from many perspectives and the recently applied technology of constructed wetlands is being used in the treatment of eutrophic water. However, process-based models to simulate their performance are scarce, so in this work a mechanistic model was developed to simulate the removal of total suspended solids, phytoplankton and total phosphorus in free water surface constructed wetlands treating eutrophic water. The model represents the influence of the main factors of the biotope and biota on these water quality variables, and particular attention is paid to resuspension produced by wind and by avifauna. Likewise, the effect of emergent vegetation cover in sedimentation, resuspension and phytoplankton growth is included. Phytoplankton is considered to store phosphorus internally in order to use it when growing, and the contribution of phytoplankton concentration to the suspended solids budget is included. The software AQUASIM was used to calibrate and validate the model in two full-scale constructed wetlands treating eutrophic water from Lake l´Albufera de València (Spain) for three years. The simulated data and field measurements showed satisfactory adjustments for the three studied variables. The budgets obtained for each variable reveal that sedimentation and resuspension are the main processes in total suspended solids performance.

Sedimentation of organic particulate phosphorus is the most important process in total phosphorus removal. The sum of the effect of resuspension by avifauna and by wind increases by more than 50% the quantity of solids that enters the water column. The model reveals that simulating the effects of the emergent vegetation cover and resuspension is crucial for representing the performance of the studied variables.

Key words: suspended solids, phosphorus, phytoplankton, modelling, constructed wetland, avifauna.

1. Introduction

Loss of water quality in natural water bodies has become a major environmental problem for decades and many initiatives aimed at recovering good environmental status have been carried out. Eutrophication is one of the most globally widespread problems and it is considered one of the main stressors on lakes (Ballatore and Muhandiki, 2002). In eutrophic water bodies, turbidity is a critical parameter that needs to be controlled in order to recover submerged aquatic vegetation and biodiversity (Scheffer et al., 1993).

This issue has been approached from a wide range of perspectives, such as the termination of untreated sewage discharges or the improvement in wastewater treatment techniques. In other cases, eutrophic waters have been treated by using different engineered bioremediation technologies, including constructed wetlands (CWs) (Coveney et al., 2002; Wu et al., 2010).

The modelling of CW performance was initiated with the development of first-order decay models (Kadlec and Knight, 1996; Stone et al., 2004), which were based on

input/output data and the treatment processes were considered as a figurative black box. These models were simplifications of the complex wetland processes and more knowledge was needed in order to optimize the performance of CWs. Accordingly, multiple experiments and research have been carried out and a greater level of understanding has been achieved, partly due to the development of mechanistic or process-based models (Min et al., 2011). Mechanistic models use mathematical formulation to represent the processes that affect each variable inside a CW and are useful to clarify which are the key processes and how they work in CW performance.

An intermediate model between these two types is the autobiotic model developed by Kadlec (1997), which provides a low-level mechanistic explanation of phosphorus removal processes in CWs by using a first order biomass-based rate.

Over the last two decades, a great leap forward in mechanistic models for CWs has taken place (Meyer et al., 2015). Most of them were applied to simulate urban wastewater treatment in subsurface flow CWs (SSFCWs), e.g. Constructed Wetlands 2D (CW2D) (Langergraber, 2001) and Constructed Wetland Model number 1 (CWM1) (Langergraber, et al., 2009), which are based on the mathematical formulation of the Activated Sludge Model series (ASMs) (Henze et al., 2000). Mburu et al., (2012) implemented CWM1 in AQUASIM and one of the most widely used application of models CW2D and CWM1 is the Wetland Module in HYDRUS software (Langergraber and Simunek, 2012). The model FITOVERT (Giraldi et al., 2010) also uses a biochemical module based on ASMs for simulating organic matter and nitrogen in SSFCWs. Likewise, a high level of detail is achieved, e.g. BIO_PORE model (Samsó and Garcia, 2013) is able to simulate biofilm growth and clogging in porous media.

On the other hand, RWQM1 (Reichert et al., (2001)) is a mechanistic model also based on the structure of ASMs models where microalgae performance is simulated in rivers.

Nevertheless, mechanistic models developed for free water surface constructed wetlands (FWSCWs) are less numerous, and those models developed for SSFCWs or river water quality cannot be directly used in these systems. Mulling (2013) deeply studied suspended particles removal in FWSCWs and determined the changes in the type and nature of these particles throughout the treatment. Besides physical, chemical and biological processes, FWSCWs maximize the interactions with the environment and the biota. In particular, some of the most influential factors in FWSCWs are related to wind action and bioturbation (Onandia et al. 2015), which are not included in the abovementioned models.

Although some mechanistic models were developed for FWSCWs, interactions with biotope and biota are not strongly studied. A remarkable advance is the modelling developed in the stormwater treatment areas of Everglades National Park where particular attention was paid to phosphorus removal (Wang and Mitsch, 2000; Min et al., 2011). Other models were developed to simulate nitrogen, phosphorus and suspended solids from non-point source pollution (Chavan and Dennett, 2008) or from urban wastewater (Wang et al., 2012).

In order to optimize eutrophic water treatment and total suspended solids (TSS) removal in FWSCWs, it is necessary to have available an appropriate mechanistic model where the main components involved are simulated.

This study aims to develop a mechanistic model for FWSCWs treating eutrophic water in order to simulate the removal of TSS and its relation to phytoplankton and total phosphorus. This work is focused on TSS because increasing water transparency is an essential factor in achieving good ecological status in water bodies. The model will facilitate an overview of the CW´s performance within its environment since interactions with biota and biotope are included. For this reason, the model is calibrated

and validated in two full-scale FWSCWs treating hypertrophic water (named FG1 and FG2). These FWSCWs are located in *Tancat de la Pipa,* a protected area near the eutrophic shallow Lake l´Albufera de València (Spain), where the high concentration of total phosphorus (TP) and TSS hinder the recovery of the good environmental status of the water body.

This model will increase the understanding about the different processes that affect suspended solids, phytoplankton and total phosphorus by bringing to light how they work and to what extent they affect concentrations. In addition, the model could be used as a management and design tool to improve FWSCW´s performance.

2. Methods

In this section a full appraisal of the mechanistic model is presented. Furthermore, the study site where the calibration and validation were carried out is described and the sensitivity analysis is set forth in detail.

2.1. Model description

The proposed model is implemented in the software AQUASIM (Reichert, 1998). The model structure is based on processes reactions which are included in the software as dynamic processes. Components of the model are introduced as state variables and the rest of parameters are introduced as programme, constant, real list or formula variables. The mixed reactor compartment configuration is used and defined by the volume of the wetland, active variables, active processes, initial conditions and inputs. The variable-order Gear integration technique is used to solve the differential equations (Reichert, (1998)).

The model describes the processes, kinetics and stoichiometric coefficients that determine the performance of each component. The mass balance for each component is calculated by Eq. 1:

$$\frac{d(VC_n)}{dt} = Q_{in}C_{in,n} - Q_{out}C_n + Q_{rf}C_{rf,n} \pm Q_{et}C_{et,n} \pm Q_{gr}C_{gr,n} + Vr_nC_n \quad (1)$$

where n=1,2…m, *m* is the total number of components, V (L) is the water volume, t (s) is time, C_n (mg L^{-1}) is the outlet concentration of the component *n*, Q_{in} (L s^{-1}) is the inlet flow, $C_{in,n}$ (mg L^{-1}) is the inlet concentration of the component *n*, Q_{out} (L s^{-1}) is the outlet flow, Q_{rf} (L s^{-1}) is the direct rainfall flow entering to the system, $C_{rf,n}$ (mg L^{-1}) is the concentration in the rainfall of the component *n*, Q_{et} (L s^{-1}) is the flow that leaves the system due to evapotranspiration, $C_{et,n}$ (mg L^{-1}) is the concentration in the evapotranspiration of the component *n*, Q_{gr} (L s^{-1}) is accounting for the gains or losses of the system by percolation to groundwater, $C_{gr,n}$ (mg L^{-1}) is the concentration in the percolation flow of the component *n* and r_n (d^{-1}) is the reaction rate for the component *n*. Concentration of the component *n* in the evapotranspiration flow is assumed to be equal to zero. r_n is calculated as shown in Eq. 2:

$$r_n = \sum_{j=1}^{R} \upsilon_{n,j} r_j \quad (2)$$

where *j*=1,2…R, R is the total number of processes, $\upsilon_{n,j}$ is the stoichiometric factor for component *n* and process *j*, and r_j (d^{-1}) is the reaction rate for process *j*.

Components included in the model are shown in Table 1. Phytoplankton was included in order to study the contribution of its dry weight to the TSS budget and due to its relevance in the eutrophication process, and phosphorus was introduced because its

particulate forms are linked to the performance of TSS and it is usually the limiting nutrient in eutrophic water.

Table 1. Description of the components included in the model.

Component	Description	Unit
TIP	Total inorganic phosphorus.	mg P L^{-1}
OP	Organic phosphorus.	mg P L^{-1}
P_{int}	Phosphorus accumulated inside the phytoplankton cells.	mg P mg Chl a^{-1}
X_P	Phytoplankton biomass.	mg Chl *a* L^{-1}
X_{TSS}	Total suspended solids.	mg dw L^{-1}

The component X_P represents the entire phytoplankton biomass and TP was calculated as shown in Eq. 3, where i_{PXp} (mg P mg Chl a^{-1}) is the content of phosphorus in phytoplankton tissues:

$$TP = TIP + OP + P_{int} \cdot X_P + X_P \cdot i_{PXp} \quad (3)$$

Phosphorus is divided into organic and inorganic forms. OP concerns both particulate and dissolved forms and is subjected to the mineralization process (Figure 1). Inorganic phosphorus is divided into DIP (dissolved inorganic phosphorus) and PIP (particulate inorganic phosphorus) through adsorption/desorption equilibrium processes, which are linked to X_{TSS} concentration depending on the partition coefficient (K_d, L mg^{-1}) (Eq. 4). Luxury uptake of phosphorus is considered so X_P stores DIP intracellularly following the mathematical expression used by Onandia et al. (2015). The capacity of X_P for internal phosphorus storage is limited, so DIP uptake will only occur when P internally stored (P_{int}) is lower than the maximum storage capacity. Afterwards, P_{int} is used to form cellular tissue when phytoplankton grows. When X_P decays, its content of phosphorous (i_{PXp} and P_{int}) is released into the water column. Following the kinetic rate

for internally stored compounds in ASM2 (Henze et al., 2000), the release of P_{int} is modelled as an individual process. Diffusion of DIP occurs between the top 10 cm of sediment layer and water column. It was modelled by modifying Fick´s first law by a coefficient of variation in the diffusion between water and sediments ($K_{difu\ sed}$) that includes the effects of porosity and tortuosity of the sediment.

X_{TSS}, OP and PIP are subjected to sedimentation and resuspension processes, and X_P is affected by sedimentation too, which are affected by emergent vegetation cover (VC).

Based on the results obtained by Paudel and Jawitz (2012), DIP uptake by emergent vegetation was decided to be excluded from the model. It was considered that the enhancement that would be achieved in model simulations was not worthwhile with the increase in model complexity and uncertainty linked to additional parameters.

$$DIP = TIP - PIP = TIP \cdot f_d = \frac{1}{1 + k_d \cdot X_{TSS}} \quad (4)$$

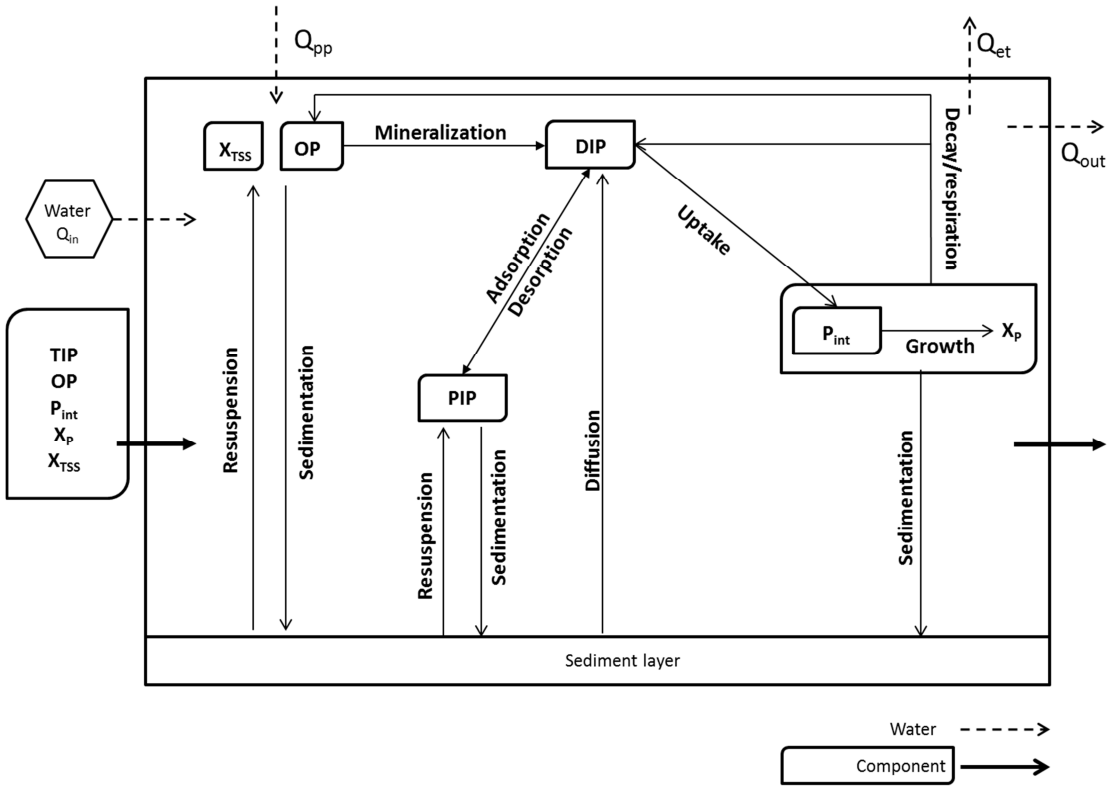

Figure 1. Schematic diagram of the model developed in this study.

Water velocity in FWSCWs is usually too low to cause resuspension so wind action is usually the most important factor involved in resuspension (Weyhenmeyer et al., 1997; Douglas and Rippey, 2000), adding bioturbation caused by avifauna and in some cases by icthyofauna (Kadlec and Wallace, 2009). Resuspension modelling varies from simple models where zero-order kinetics is used (Wang and Mitsch, 2000), to very detailed models where an exhaustive sediment characterization is needed (Chapra, 1997). In order to find the balance between process comprehensiveness and field data obtained, resuspension is divided into two independent processes: resuspension caused by wind and resuspension caused by bioturbation.

In relation to wind resuspension, a necessary condition for this process is that the wavelength of the wave caused by wind needs to have a magnitude at least double the water depth. Thereby, it is possible to obtain the minimum wind speed to cause resuspension (W_0, m s^{-1}) using an empirical equation developed for coastal oceanography that is commonly used for quantitative analyses about resuspension in shallow lakes (Nagid et al., 2001):

$$L = 1.56\left[0.77 \cdot W \cdot \tanh\left[0.077\left(\frac{9.8 \cdot F}{W^2}\right)^{0.25}\right]\right]^2 \quad (5)$$

where L (m) is wavelength, W (m s^{-1}) is wind speed and F (m) is the fetch. The fetch is the maximum distance that can be uniformly affected by speed and wind direction in a water body, and it is calculated taking into account wind direction, length and width of the FWSCW. According to the model proposed by Cózar et al. (2005) for TSS and turbidity in shallow lakes, TSS resuspension caused by wind is modelled through a correlation with daily maximum wind speed observed data (Eq. 6). Resuspension also releases P from sediment to the water column (Søndergaard et al., 1992), which depends

on the P content in the sediments (i_{Psed}, mg P mg dw^{-1}) and is added as OP or PIP depending on F_{pr} (fraction of resuspended P recycled to OP) (Eq. 7 and 8). Resuspension by wind is not a dynamic process, but it is used to calculate the concentrations that this phenomenon causes by adding sediment to the water column, so it is considered as an input to the system.

The trapping effect of particulate components by emergent vegetation is introduced in resuspension kinetics. According to Hosokawa and Horie (1992), an improvement in TSS removal was demonstrated in laboratory channels and CWs planted with *Phragmites australis*. Vegetation cover (i.e. the fraction of the CW surface covered by the projection of the aerial part of the plants) and $K_{veg\ resus}$ (coefficient for trapping by emergent VC in resuspension processes) were used to model the effect of emergent vegetation in resuspension processes through the expression $(1 - VC \cdot K_{veg\ resus})$ (Eq. 6-8). Resuspension by wind is zero when the CW surface is completely vegetated (VC=1) and is maximum when no vegetation is present (VC=0).

Equations 6-8 were used to calculate X_{TSS}, OP and PIP entering to the system by wind resuspension:

$$X_{TSS\ res}(mg\ l^{-1}) = \alpha \cdot W^{\beta} \delta(W, W_o)(1 - VC \cdot K_{veg\ resus}) \quad (6)$$

$$OP_{res}(mg\ P\ l^{-1}) = \alpha \cdot W^{\beta} \delta(W, W_o)(1 - VC \cdot K_{veg\ resus}) \cdot i_{Psed} \cdot F_{pr} \quad (7)$$

$$PIP_{res}(mg\ P\ l^{-1}) = \alpha \cdot W^{\beta} \delta(W, W_o)(1 - VC \cdot K_{veg\ resus}) i_{Psed} \cdot (1 - F_{pr}) \quad (8)$$

where W (m s^{-1}) is maximum daily wind speed, α and β are parameters to be calibrated, while $\delta(W,W_0)$ is a step function that determines the periods when the wind-induced waves cause resuspension ($\delta=0$ if $W<W_o$ and $\delta=1$ if $W>W_o$).

224 Table 2. Resuspension factor (RF_i) for the different groups of birds observed in
225 FWSCWs.

RF	Description	Examples of species
10	Large birds that actively remove the substrate to feed.	*Phoenicopterus spp.*
9	Medium-sized birds that actively remove the substrate to feed.	*Platalea leucorodia*
8	Large fishing birds that remove the substrate.	*Phalacrocorax carbo*
7	Medium-sized waterfowl that feed on the substrate; large fisher herons.	*Anas platyrhynchos, Anas strepera, Ardea cinerea, Egretta alba, Tadorna tadorna*
6	Medium-sized waterfowl that do not feed on the substrate; herons that feed on the substrate; large waders; medium-sized waders that remove the substrate to feed.	*Anas acuta, Fulica atra, Fulica cristata, Limosa limosa, Netta rufina, Plegadis falcinellus, Recurvirostra avosetta*
5	Fisher herons; large size rallids; diving waterfowl that feed on the substrate.	*Ardea purpurea, Aythya ferina, Porphyrio porphyrio*
4	Small waterfowl that feed on the surface; waders and medium-sized rallids.	*Anas clypeata, Anas crecca, Anas penelope, Anas querquedula, Gallinula chloropus, Himantopus himantopus, Philomachos pugnax, Tringa erythropus, Tringa nebularia, Tringa stagnatilis, Vanellus vanellus*
3	Medium-sized fisher herons; medium and large swimming birds that do not remove the substrate; medium-sized fisher herons; great diving waterfowl that do not feed the substrate.	*Ardeola ralloides, Botaurus stellaris, Bubulcus ibis, Egretta garzetta, Ixobrychus minutus, Larus audouinii, Larus fuscus, Larus michahellis, Nycticorax nycticorax, Podiceps cristatus*
2	Waterfowl divers that do not feed on the substrate.	*Podiceps nigricollis, Tachybaptus ruficollis*
1	Small waders; swimmer birds that do not remove the substrate.	*Actitis hypoleucos, Calidris alpina, Calidris ferruginea, Calidris minuta, Calidris temminckii, Charadrius alexandrinus, Charadrius dubius, Charadrius hiaticula, Gallinago gallinago, Larus genei, Larus ridibundus, Lymnocryptes minimus, Porzana parva, Rallus aquaticus, Tringa glareola, Tringa ochropus, Tringa totanus*
0	Fishing birds that only affect waterbodies for fishing hauls; aquatic birds that do not feed or rest on it.	*Chlidonias hybrida, Chlidonias leucopterus, Chlidonias niger, Gelochelidon nilotica, Glareola pratincola, Mycteria ibis, Sterna hirundo, Sternula albifrons*

226

227 With regard to resuspension caused by bioturbation, bird activity is an influencing
228 factor in sediment resuspension that increases TSS concentration in CWs (Greenway,
229 2010; Martin et al., 2013). The amount of resuspension produced depends on the
230 density and type of birds. Field observations reveal that some groups of birds such as
231 passerine birds, that are small and light, have no impact on water quality. Others like
232 flamingo (*Phoenicopterus spp*.) cause considerable sediment resuspension due to
233 filtering action while feeding (Comín et al., 1997; Glassom and Branch, 1997).
234 According to these observations, avifauna is divided into different groups of birds (i)
235 depending on their affection to sediment resuspension and consequently a resuspension
236 factor (RF_i) is assigned to each group (Table 2). This classification takes into account
237 bird size, feeding habits and ways of movement within the CW in order to estimate their
238 impact on sediment resuspension.
239 The effect of vegetation cover in avifauna resuspension is modelled as in resuspension
240 caused by wind.
241 Before introducing a mathematical expression for modelling resuspension caused by
242 icthyofauna, an estimation of the magnitude of this process in *Tancat de la Pipa*, the
243 area where the model was calibrated and validated, was carried out. The highest density
244 of fishes was detected in the so-called *Reserve Lagoon* (Figure 1), where 33.33 kg ha^{-1}
245 were counted in April 2014, mainly *Cyprinus carpio* (data not published). Considering
246 that $77.24 \cdot 10^{-4}$ mg L^{-1} of TSS can be resuspended per each kg of *Cyprinus carpio*
247 contained in one hectare (Tsanis et al., 1998), it was calculated that 0.26 mg L^{-1} of TSS
248 could be resuspended by icthyofauna. Comparing with average TSS concentrations in
249 *Tancat de la Pipa* (Martin et al, 2013), this quantity means less than 2% of TSS entering
250 and leaving these FWSCWs. Given the low impact of icthyofauna resuspension in the

system where the model was calibrated and validated, this process was not included in the model.

Influence of vegetation cover on sedimentation processes of X_{TSS} and the particulate fractions of TIP and OP was described using the expression $(1 + VC \cdot K_{veg\ sed})$, where $K_{veg\ sed}$ is the coefficient for trapping by emergent VC in sedimentation processes. The higher the vegetation cover, the greater the effect of trapping.

Regarding phytoplankton biomass, it is usually measured as the concentration of chlorophyll *a* and its contribution to TSS concentration depends on its ratio dry weight:Chl *a* (i_{TSSXp}). Light limitation in phytoplankton growth kinetics (G_L) is simulated as described in Di Toro et al., (1971), where diurnal surface-light variation, light attenuation with depth and photoinhibition are included. Emergent vegetation cover is taken into account in order to model its influence in incident daylight intensity (Eq. 9). Spatial variation of light down through the water column is modelled by the Beer-Lambert law and the extinction coefficient is determined in accordance to X_P concentration (Eq. 10).

$$G_L = \frac{2.718 \cdot f}{k_e \cdot H}\left(\exp\left(-\frac{I_0}{I_s}e^{-k_e \cdot H}\right) - \exp\left(-\frac{I_0}{I_s}\right)\right) \cdot (1 - VC) \quad (9)$$

$$K_e = K_{e0} + a_{Xp} \cdot X_P \quad (10)$$

where f is the photoperiod (the fraction of daylight), K_e (m^{-1}) is the extinction coefficient, H (m) is water depth, I_0 (ly d^{-1}) is the average incident daylight intensity, I_s (ly d^{-1}) is the saturating light intensity, K_{e0} (m^{-1}) is the light attenuation coefficient of water and a_{Xp} (L mg^{-1} m^{-1}) is the specific light attenuation coefficient of phytoplankton.

Temperature influences OP mineralization, DIP diffusion, growth, decay and respiration of phytoplankton, and it is simulated with the Arrhenius equation (Eq. 11).

$$k_T = k_{20}\theta^{T-20} \quad (11)$$

where k_T (d^{-1}) is process rate at temperature T, k_{20} (d^{-1}) is process rate at 20ºC, θ is temperature coefficient and T (ºC) is temperature.

Processes described in Table 3 are dynamic processes, while adsorption/desorption is a chemical equilibrium process that determines the relation between the measured component DIP and the calculated component PIP, in accordance with the partitioning coefficient, K_d.

Parameters used are given in Appendix A.

283

Table 3. Stoichiometric matrix and processes rates in the model.

	Component → Process ↓	TIP	P_{int}	OP	X_P	X_{TSS}	r
1.	Mineralization of OP	1		-1			$K_{min\,OP}\theta_{min\,OP}^{T-20}\left(\frac{DO}{DO+k_{DO}}\right)OP$
2.	Phosphorus uptake by X_P	$-X_P$	1				$P_{max\,uptake}\left(\frac{P_{max}-P_{int}}{P_{max}-P_{min}}\right)\left(\frac{TIP\cdot f_d}{k_{DIPup}+TIP\cdot f_d}\right)$
3.	Growth of X_P		$-i_{PXp}/X_P$		1	i_{TSSXp}	$G_{max}\theta_G^{T-20}\left(\frac{P_{int}-P_{min}}{P_{max}-P_{min}}\right)X_P\cdot G_L$
4.	Decay of X_P	$i_{PXp}\,(1-F_{op})$		$i_{PXp}\cdot F_{op}$	-1	$-i_{TSSXp}$	$K_r\theta_r^{T-20}X_P$
5.	Lysis of P_{int}	X_P	-1				$K_r\theta_r^{T-20}P_{int}$
6.	Respiration of X_P	$i_{PXp}\,(1-F_{op})$		$i_{PXp}\cdot F_{op}$	-1	$-i_{TSSXp}$	$K_{resp}\theta_{resp}^{T-20}\frac{DO}{k_{DO\,Xp}+DO}X_P$
7.	Sedimentation of X_P				-1	$-i_{TSSXp}$	$\left(\frac{v_{sXp}}{H}\right)X_P$
8.	Sedimentation of X_{PIP}	-1					$\left(\frac{v_{sTIP}}{H}\right)TIP(1-f_d)(1+VC\cdot K_{veg\,sed})$
9.	Sedimentation of OP			-1			$\left(\frac{v_{sOP}}{H}\right)OP\cdot f_{POP}(1+VC\cdot K_{veg\,sed})$
10.	Sedimentation of X_{TSS}					-1	$\left(\frac{v_{sTSS}}{H}\right)X_{TSS}(1+VC\cdot K_{veg\,sed})$
11.	Resuspension by avifauna	$i_{Psed}\cdot(1-F_{pr})$		$i_{Psed}\cdot F_{pr}$		1	$K_{avi}\frac{\sum_{i=0}^{i}N_i\cdot RF_i}{A}(1-VC\cdot K_{veg\,res})$
12.	Diffusion	1					$D_{0P}\cdot K_{difu\,sed}\cdot\theta_{difu}^{T-20}(P_{sed}-PIT\cdot f_d)\frac{1}{0.1\cdot H}$

2.2. Study site and experimental data

The developed model was applied on the FWSCWs situated in *Tancat de la Pipa*, which is located at 39°21´51´´N-0°20´47´´O in Valencia, Spain. This set of CWs treats eutrophic fresh water from the adjacent lake known as L´Albufera and is divided into different units (Figure 2). Water continuously enters the FWSCW named as FG1 from point P0 and moves by gravity flow. FWSCWs FG1 (13509 m^2) and FG2 (18240 m^2) work in series and in both cases, water flows through four sluices of 0.3 m width, spaced every 30 m. Water depths in both systems remain between 0.15-0.25 m. Percolation was demonstrated to be negligible (Martin et al., 2013). Both units were planted with cattails in January-February 2009, with a density of 1 stem m^{-2}. FG1 was harvested in October 2009, vegetation cover in FG2 started to drop in May 2010 and emergent vegetation was not recovered in any unit.

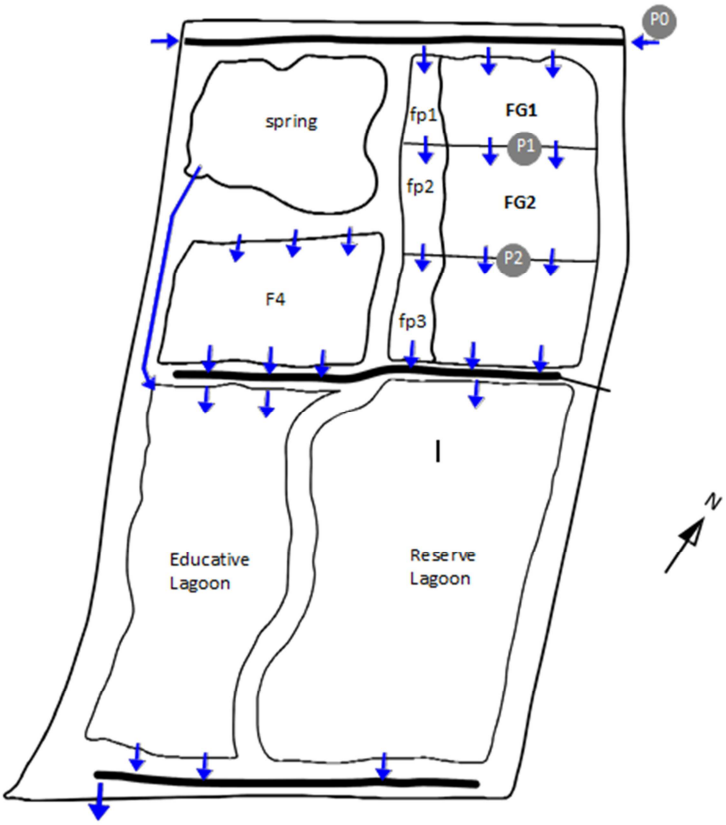

Figure 2. Schematic representation of the study site.

298 Monitoring was carried out from April 2009 to April 2012. During this period the
299 system was operated with hydraulic loading rates (HLR) between 26 and 209 m $year^{-1}$.
300 The inlet was interrupted during October-November 2009, March and August 2011 due
301 to maintenance operations. More details about the FWSCWs configuration and
302 operation can be seen in Martín et al. (2013).
303 Hydraulic monitoring was carried out by measuring water depths and velocities in each
304 inlet sluices. Gauging sections consist of rectangular sections where free surface flow
305 exists and velocities are gauged with a mini current meter (Rivers-Moore et al., 2006).
306 Water samples were collected in points P0, P1 and P2 every two weeks since April
307 2009 to October 2011, and monthly from November 2011 to April 2012 (n=64). These
308 samples were analysed for total suspended solids (TSS), chlorophyll *a* (Chl *a*), total
309 phosphorus (TP), phosphates (PO_4^{3-}-P) and total and soluble chemical oxygen demand
310 (TCOD and SCOD) (Martin et al., 2013).
311 They were collected between 9.00 h and 14.00 h at a depth of 0.1 m with 2L bottles,
312 transported and preserved at 4ºC until analysis took place, no later than 24h after
313 sampling. In all these samples TP and PO_4^{3-}-P were analysed using the Spectroquant®
314 Analysis System by Merck, TSS was determined according to APHA (1991) and Chl *a*
315 was obtained by extracting photosynthetic pigments using acetone 90% as solvent,
316 absorbance values were determined with a spectrophotometer, and by using the
317 equations devised by Jeffrey and Humphrey (1975). Dissolved oxygen (DO),
318 conductivity, pH and temperature were measured *in situ* using portable field
319 measurement equipment (WTW-Multi 340i).
320 Following Eq. 3, phosphorus fractioning in the water samples was carried out: DIP
321 concentration was assumed to be measured phosphates, OP was equivalent to 1% of
322 TCOD, P_{int} was assumed to be equal to P_{min} and PIP was calculated as the difference

between TP and the rest of fractions. Initial conditions for the components concentrations are showed in Table 4:

Table 4. Initial conditions for the component concentrations in FWSCWs FG1 and FG2.

Component	Units	Initial conditions	
		FG1(calibration)	FG2 (validation)
TIP	mg P L^{-1}	0.401	0.073
OP	mg P L^{-1}	0.029	0.030
P_{int}	mg P mg Chl a^{-1}	0.520	0.520
X_P	mg Chl *a* L^{-1}	0.007	0.001
X_{TSS}	mg L^{-1}	16.5	10.1

Phosphorus content in sediments (i_{Psed}) was measured by extracting P with $HNaCO_3$ and analysing the extract by spectrophotometric method based on phosphate-molybdate complex (ISO 11263:1994).

Rainfall and evapotranspiration data were obtained from a nearby meteorological station located in Picassent (10 km west of FWSCWs), which belongs to a national agricultural research centre (IVIA, http://riegos.ivia.es/). Data related to wind (mean speed, maximum speed and wind direction), photoperiod and average incident daylight intensity were also obtained from this station. The fetch was calculated considering that the FWSCWs are orientated in a NW direction, that the prevailing wind direction observed in the meteorological station is East (29%) and that resuspension occurs in any point of the water body. The fetch was established to be the half of the width: 72 m in FG1 and 80 m in FG2. Using Eq. 5, W_0 was calculated to be 3.2 m s^{-1} in FG1 and 2.5 m s^{-1} in FG2.

The abundance of each waterfowl species in the FWSCW was counted every two weeks from September 2009 to April 2012. Censuses were performed using a telescope during the first three hours after sunrise and during each session the same transect was surveyed; several observation points were traced in order to ensure a complete census in the CWs.

346 Emergent vegetation cover was estimated through fortnightly *in situ* observation and
347 aerial images examination.
348 In order to implement the developed model in FG1 and FG2 FWSCWs, the hydraulic
349 operation of the systems needed to be simulated. A water mass balance was used for
350 accomplishing this aim but with no deeper purpose.
351 Each FWSCW was modelled as a non-dimensional element and therefore the
352 components presented uniform values in the entire compartment and in the outlet.
353 Following Harter and Mitsch (2003), the hydraulic sub-model was based on site data
354 and it was not altered for any of the simulations. The water mass balance was calculated
355 by the dynamic water budget approach and changes in the water volume were strictly
356 due to changes in the water depth:

$$Q_{out} = Q_{in} + Q_{rf} - Q_{et} \pm Q_{gr} - \frac{dV}{dt} \quad (12)$$

357

358 **2.3. Calibration and validation of the model**

359 Calibration was carried out in FG1 FWSCW and validation in FG2 FWSCW.
360 Calibration of model parameters was carried out by adjusting their values in order to
361 obtain the best fit between simulated and observed data (April 2009-April 2012).
362 The suitability of the hydraulic operation representation was determined by using the
363 conservative variable conductivity as a natural tracer since its concentration is not
364 affected by any reactive process and its evolution can be directly linked to the hydraulic
365 performance of the system (Schmidt et al., 2012). Eq. 1 and 12 were applied to
366 conductivity in order to obtain simulated values. The goodness of the adjustment
367 between observed and simulated values was evaluated using the Nash-Sutcliffe
368 efficiency coefficient (NSE, Eq. 13). Values between 0.0 and 1.0 are generally

considered as acceptable adjustments while values lower than 0.0 indicate that the residual variance obtained from simulated data is greater than the data variance.

$$\mathrm{NSE} = 1 - \left[\frac{\sum_{i=1}^{n}(Y_i^{obs} - Y_i^{sim})^2}{\sum_{i=1}^{n}(Y_i^{obs} - Y_i^{mean})^2}\right] \quad (13)$$

where Y_i^{obs} and Y_i^{sim} are the *i*th datum for the observed and simulated value and Y^{mean} is the mean of the observed data.

The value of the root mean square error (RMSE, Eq. 14) was used to evaluate the adjustment of the model by comparing simulated and observed outlet concentrations:

$$\mathrm{RMSE} = \sqrt{\frac{\sum_{i=1}^{n}(Y_i^{obs} - Y_i^{sim})^2}{n}} \quad (14)$$

where *n* is the total number of observations.

2.4. Sensitivity analysis

The sensitivity of the developed model was studied in order to find out the most influential parameters in output concentrations of the components. It was carried out in AQUASIM, where linear sensitivity functions of arbitrary variables are calculated with respect to each of the parameters included in the analysis (Reichert, 1998). The absolute-relative sensitivity ($\delta_{y,p}^{a,r}$) function of AQUASIM was used (Eq. 15), which measures the absolute change is an arbitrary variable calculated by AQUASIM, *y*, for a 100% change in any parameter of interest, *p*. This makes quantitative comparisons of the different parameters on a common variable possible. The 33 parameters included in the stoichiometric matrix were studied.

$$\delta_{y,p}^{a,r} = p\frac{\partial y}{\partial p} \quad (15)$$

3. Results and discussion

In this section the results from the calibration and validation of the developed model in FG1 and FG2 units are shown and analysed. Observed and simulated values from April 2009 to April 2012 are compared.

3.1. Representation of the hydraulic operation

Firstly, the hydraulic operation of both systems was simulated. Outlet flow from FG1 and FG2 was calculated by applying the water mass balance depicted in Eq. 12. The conservative variable conductivity was modelled and a satisfactory adjustment between observed and simulated data was obtained (Figure 3a). NSE presented a value of 0.85 in FG1 and 0.57 in FG2. The obtained hydraulic retention times (HRT) followed the same pattern in both units, reaching the highest values (7.2 d) during the first months of simulation (Figure 3b). Mean value of HRT was 1.0 d in FG1 and 1.3 d in FG2.

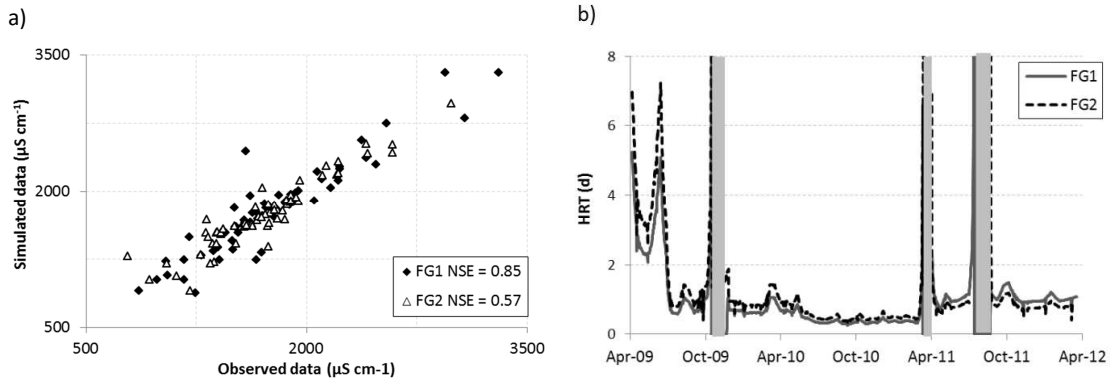

Figure 3. a) Comparison between observed and simulated conductivity values. b) Calculated hydraulic retention time (HRT, d). Grey vertical bars indicate dry periods.

3.2. Calibration and validation results

A set of parameter values that allow good fits between observed and simulated X_{TSS}, X_P and TP outlet concentrations was achieved, although there is insufficient evidence to support that this is the only possible set.

The first step was to calibrate α and β, which are parameters related to wind resuspension. A power function (Figure 4a) was fitted to observed TSS values in FG1 unit, finding that 40 mg L^{-1} is the background concentration which is not related to wind resuspension, $\alpha=6\cdot10^{-6}$ and $\beta=7.4$. When comparing these values with those obtained by Cózar et al. (2005) ($\alpha=0.0405$, $\beta=2.58$) it is observed that α is lower than that obtained in their study and the calibrated value of β is in the same order of magnitude.

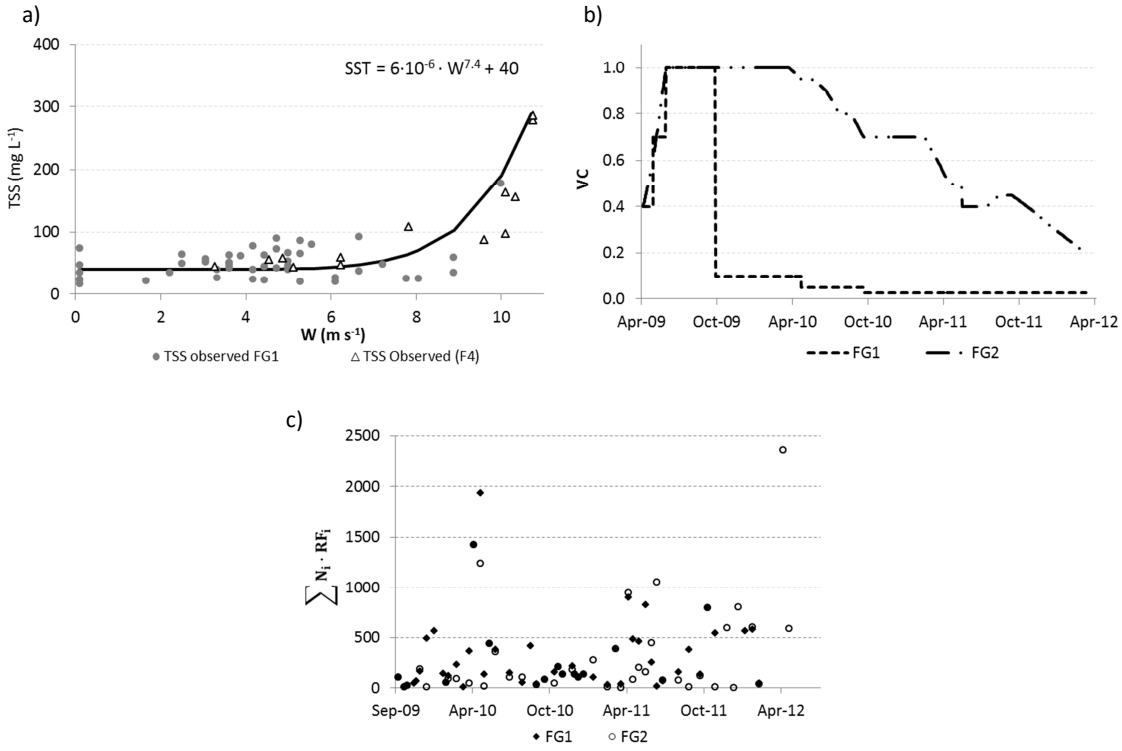

Figure 4. a) Correlation between maximum daily wind speed and TSS concentration in FG1, from April 2009 to April 2012. Circles represent outlet concentrations from FG1 and triangles from the adjacent CW F4 (see Figure 1). b) Emergent vegetation cover in FG1 and FG2. c) Sum of the number of birds (N_i) multiplied by its resuspension factor (RF_i) in FG1 and FG2.

Afterwards, values given to parameters K_{avi}, $K_{veg\ sed}$ and $K_{veg\ resus}$ were chosen based on our previous experiences, since they were published for the first time in this model and bibliographic reference values are not available. The other parameters were initially used with the most common values found in bibliography and some of them needed to be modified in order to get the best fitting results (Table 5). Figure 4c shows that bird

pressure in both FWSCW is lower in summer and winter and higher in spring, when surrounding fields are dried and birds move to *Tancat de la Pipa* for feeding, resting and reproduction.

X_{TSS} content in X_P was calculated using the values stated by Reynolds (2006) for different phytoplankton species in freshwater and the composition of the phytoplankton community in *Tancat de la Pipa* determined by Calero et al. (2015). A value of 14.6 mg Chl *a* g dw^{-1} was calculated (i.e. i_{TSSXp} = 68.49 mg dw mg Chl *a* $^{-1}$), which is in the middle of the range 3-39 mg Chl *a* g dw^{-1} determined by Reynolds (2006). Following Baretta-Bekker et al. (1997), P_{max} was established to be double the value of i_{PXp} while P_{min} was half the value.

Regarding i_{Psed}, the average concentration measured in laboratory analyses was $1.43 \cdot 10^{-4}$ mg P mg dw^{-1}. Phosphorus concentration in interstitial water in sediments was considered to be the average value of the measurements carried out by Martín (1998) in Lake Albufera sediments (P_{sed} = 2.96 mg P L^{-1}).

The fraction of particulate organic phosphorus was calculated as the fraction between particulate and total chemical oxygen demand. Calibration of dissolved and particulate fractions of inorganic phosphorus carried out in FG1 set the value of K_d in 0.19 L mg^{-1}. However, this value could not be validated in the system FG2 because it generated simulated values lower than those observed and high values of RMSE. For these reasons, a different value of K_d was used in FG2 (0.07 L mg^{-1}). This variation in partition coefficient for inorganic phosphorus could be due to differences in the adsorptive properties of the TSS in these systems.

453 Table 5. Values of the parameters and stoichiometric coefficients.

Parameter	Description	Value	Source
a_{Xp}	Specific light attenuation coefficient of phytoplankton (L mg^{-1} m^{-1}).	8.8	Chapra, 1997
D_{0P}	Diffusion coefficient of DIP (m^2 d^{-1}).	$6.34 \cdot 10^{-5}$	Reddy and DeLaune, 2008
F_{op}	Fraction of P recycled to OP in X_P decay.	0.8	Martin, 1998
f_{POP}	Fraction of particulate organic phosphorus.	0.34	This study
F_{pr}	Fraction of resuspended P recycled to OP.	0.5	This study
G_{max}	Maximum growth rate for X_P at 20 ºC (d^{-1}).	2	Ambrose et al. 1988
i_{PXp}	P content ratio in X_P (mg P mg Chl a^{-1}).	1.04	This study
i_{TSSXp}	TSS content ratio in X_P (mg dw mg Chl a^{-1}).	68.49	This study
I_s	Saturating light intensity for X_P (ly d^{-1}).	150	This study
K_{avi}	Coefficient of resuspension by avifauna (mg m^2 L^{-1} d^{-1}).	1081	This study
K_d	Partition coefficient for inorganic phosphorus (L mg^{-1}).	0.07 - 0.19	This study
k_{DIPup}	Saturation coefficient for DIP in P uptake by X_P (mg P L^{-1}).	0.0005	This study
$K_{difu\ sed}$	Coefficient of variation in the diffusion between water and sediments.	0.4	This study
k_{DO}	Saturation coefficient for DO in OP mineralization (mg O_2 L^{-1}).	2.0	This study
$k_{DO\ Xp}$	Saturation coefficient for DO in X_P respiration (mg O_2 L^{-1}).	0.2	Reichert et al., 2001
K_{e0}	Light attenuation coefficient of water (m^{-1}).	0.1	This study
$K_{min\ OP}$	OP mineralization rate at 20ºC (d^{-1}).	0.22	Ambrose et al. 1988
K_r	X_P decay rate at 20 ºC (d^{-1}).	0.1	Reichert et al., 2001
K_{resp}	X_P respiration rate at 20 ºC (d^{-1}).	0.1	Reichert et al., 2001
$K_{veg\ resus}$	Constant for trapping by emergent VC in resuspension processes.	0.1	This study
$K_{veg\ sed}$	Constant for trapping by emergent VC in sedimentation processes.	9.0	This study
P_{max}	Maximum P_{int} concentration (mg P mg Chl a^{-1}).	2.08	Baretta-Bekker et al. 1997
$P_{max\ uptake}$	Maximum phosphorus uptake rate (mg P mg Chl a^{-1} d^{-1}).	1.28	Onandia et al., 2015
P_{min}	Minimum P_{int} concentration (mg P mg Chl a^{-1}).	0.52	Baretta-Bekker et al. 1997
v_{sOP}	Sedimentation velocity of OP (m d^{-1}).	0.07	This study
v_{sTIP}	Sedimentation velocity of TIP (m d^{-1}).	0.04	This study
v_{sXTSS}	Sedimentation velocity of X_{TSS} (m d^{-1}).	0.07	This study
v_{sXp}	Sedimentation velocity of X_P (m d^{-1}).	0.07	This study
α	First coefficient of resuspension by wind.	$6 \cdot 10^{-6}$	This study
β	Second coefficient of resuspension by wind.	7.4	This study
θ_{difu}	Temperature coefficient for DIP diffusion.	1.0234	Reddy and DeLaune, 2008
θ_G	Temperature coefficient for X_P growth.	1.068	Ambrose et al. 1988
$\theta_{min\ OP}$	Temperature coefficient for mineralization of OP.	1.08	Ambrose et al. 1988
θ_r	Temperature coefficient for X_P decay.	1.02	Ambrose et al. 1988
θ_{resp}	Temperature coefficient for X_P respiration.	1.045	Ambrose et al. 1988

454

Figures 5, 6 and 7 show the relationships between observed and simulated data for X_{TSS}, X_P and TP in FG1 (calibration) and FG2 (validation). Calibration results were satisfactory for the three water quality variables. Furthermore, validation in FG2 shows even better adjustment, which confers greater robustness to the model.

Lower TSS concentrations fit slightly better than higher ones, especially in FG1 where outlet concentrations above 100 mg L^{-1} were observed. Even so, a good adjustment was obtained when comparing with TSS concentration.

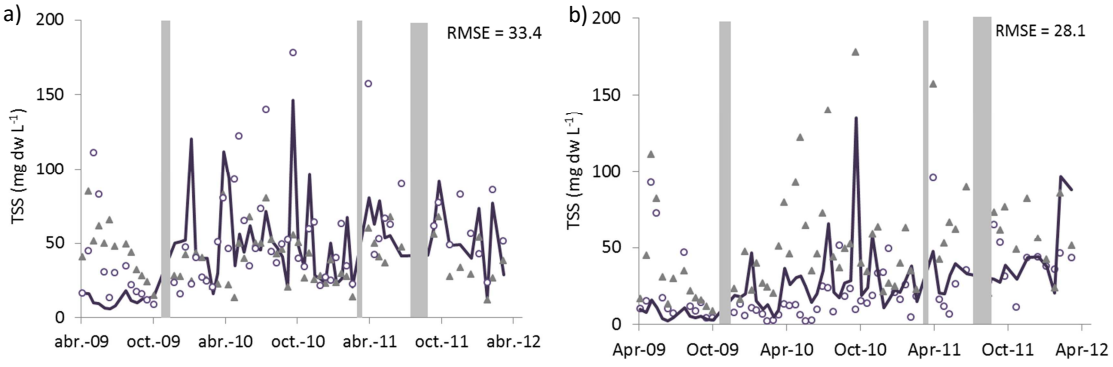

Figure 5. Comparison between observed (circles) and simulated (line) X_{TSS} outlet concentrations (mg dw L^{-1}) in (a) FG1 and (b) FG2. Triangles represent observed inlet concentrations and grey vertical bars indicate dry periods.

In relation to X_{TSS} removal, the FG1 FWSCW showed a change in its performance during the studied period since TSS removal was only achieved during the first year of operation and from then on, outlet concentrations were higher than inlet ones (Figure 5a). The model is able to successfully reproduce both trends and good adjustment is achieved during the entire studied period. The change in TSS efficiency removal that took place in FG1 from March 2010 onwards is associated with a drop in emergent vegetation cover (Figure 4b), since it was harvested in October 2009 and it did not grow again. It was proved that emergent vegetation cover is statistically related with observed TSS concentrations ($p<0.01$).

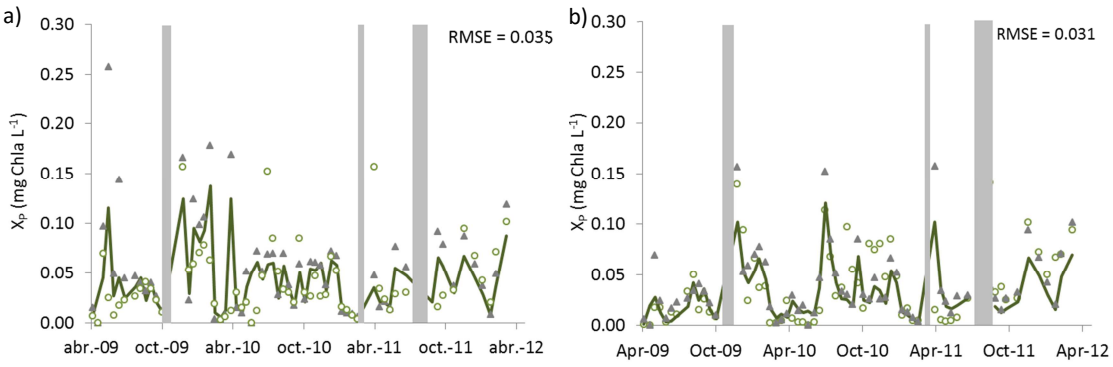

Figure 6. Comparison between observed (circles) and simulated (line) X_P outlet concentrations (mg Chl *a* L^{-1}) in (a) FG1 and (b) FG2. Triangles represent observed inlet concentrations and grey vertical bars indicate dry periods.

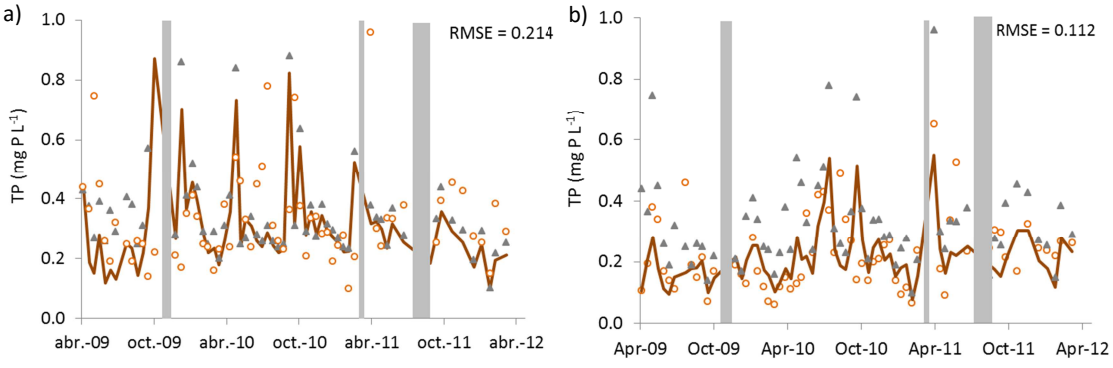

Figure 7. Comparison between observed (circles) and simulated (line) TP outlet concentrations (mg P L^{-1}) in (a) FG1 and (b) FG2. Triangles represent observed inlet concentrations and grey vertical bars indicate dry periods.

Regarding phytoplankton and total phosphorus results (Figures 6 and 7), the model properly simulates outlet concentrations in both systems.

Some simulations that did not include vegetation cover were carried out in order to clarify its significance in X_{TSS} performance. Figure 8 shows that the higher the vegetation cover, the lower the concentrations achieved. Furthermore, the developed model revealed that the magnitude of the effect of emergent vegetation in trapping particulate matter is much greater in sedimentation processes ($K_{veg\ sed}$ = 9.0) than in resuspension ones ($K_{veg\ resus}$ = 0.1).

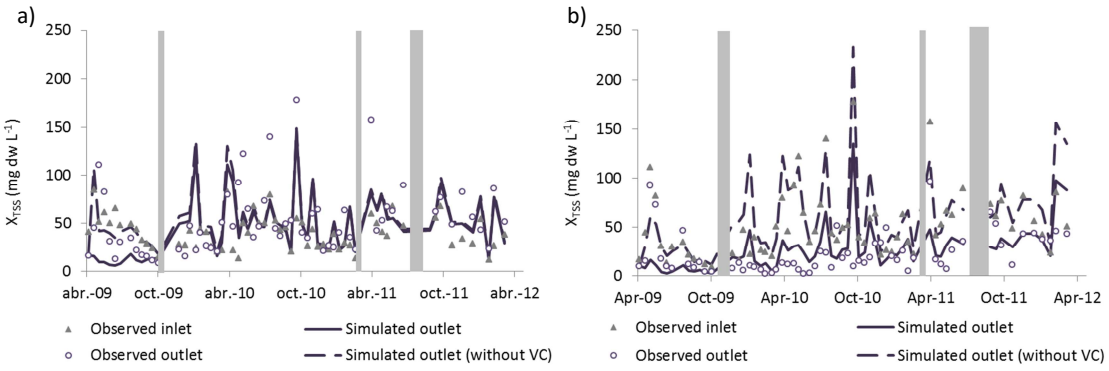

Figure 8. Simulated TSS concentrations with plant effects (solid line) and without plant effects (dotted line) in (a) FG1 and (b) FG2.

3.3. Sensitivity results

The sensitivity analysis was carried out in order to find out the influence of the parameter values over components concentrations. Table 6 depicts a classification of the most sensitive parameters for each component based on the mean absolute-relative sensitivity calculated.

Table 6. Parameter classification based on the mean absolute-relative sensitivity function in AQUASIM.

	X_{TSS}	X_P	PIT	P_{int}	OP
>1	$K_{veg\ sed}$, v_{sTSS}, K_{avi}				
>0.1-0.5<	i_{TSSXp}, v_{sXp}, $K_{veg\ resus}$, θ_{resp}, θ_r			P_{max}, θ_r, $P_{max\ uptake}$, P_{min}	
<0.1	G_{max}, K_r	θ_{resp}, θ_r, v_{sXp}, K_r, K_{resp}, θ_G, K_{avi}, I_S, f, G_{max}	$K_{veg\ sed}$, v_{sPIP}, K_d, K_{avi}	K_{avi}, θ_G, K_r, I_S, i_{PXp}, θ_{resp}, G_{max}, f	f_{POP}, $K_{veg\ sed}$, $\theta_{min\ OP}$, v_{sOP}

X_{TSS} was the most susceptible component to changes in the value of the parameters, particularly in relation to $K_{veg\ sed}$, v_{sTSS} and K_{avi}. i_{TSSXp}, v_{sXp}, $K_{veg\ resus}$, θ_{resp} and θ_r presented intermediate sensitivity for X_{TSS}, meanwhile parameters related to internal

accumulation of phosphorus and temperature coefficient for X_P decay were the most sensitive parameters for P_{int}. X_P, PIT and OP showed the lowest absolute-relative sensitivity values, and among the parameters that most affect these components are their sedimentation velocities, the coefficient for trapping by emergent VC in sedimentation processes, the temperature coefficient for X_P respiration and the fraction of particulate organic phosphorus.

3.4. Mass budgets

Few studies offer information about the relative significance of the different processes for efficient removal in FWSCWs (Wang and Mitsch, 2000). However, this is a key issue for making decisions by CW managers and this type of mechanistic models pave the way for further contributions in this area. X_{TSS}, X_P and TP budgets were calculated from simulation results in FG1 and FG2 from April 2009 to April 2012.

X_{TSS} associated to inflow represents no more than 60% of the total amount of solids that enters the studied FWSCWs (Figure 9). Inputs produced by resuspension processes caused by wind and by avifauna means 50% of TSS entering to FG1 and 44% in FG2, with a predominant importance of wind resuspension in both budgets.

In FG1 and FG2 FWSCWs sedimentation is the most influential process in X_{TSS} performance, which is consistent with observations made by Schmid et al. (2005), especially in FG2 where X_{TSS} sedimentation removes 75% of solids that comes into the system. The greater importance of sedimentation in FG2 is associated with the higher emergent vegetation cover in this system. Likewise, higher vegetation cover in FG2 explains that resuspension processes are lower in this system.

Processes related to phytoplankton are of little importance in the X_{TSS} budget. Phytoplankton dynamic affects turbidity but its contribution to X_{TSS} concentration is very low (2%, approximately).

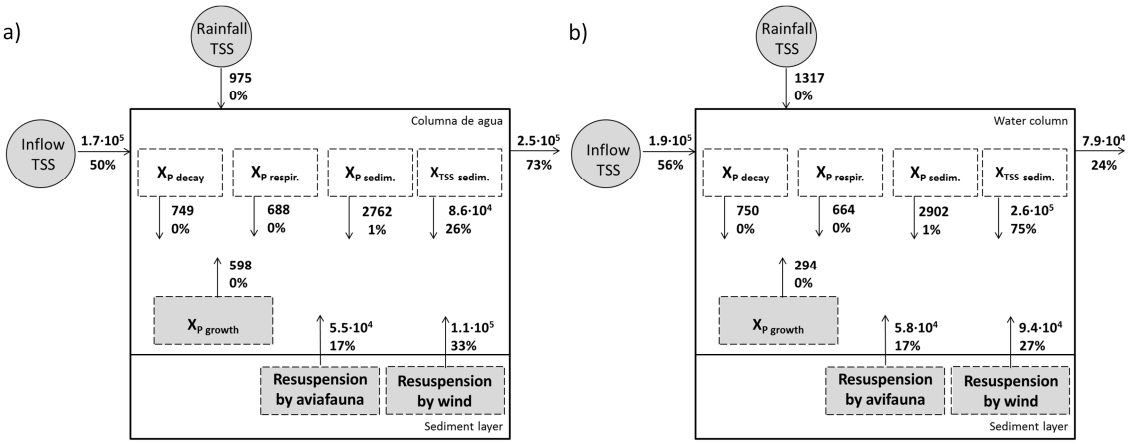

Figure 9. Total suspended solids budget (kg) for (a) FG1 and (b) FG2 as calculated from the model for April 2009-2012. Grey-coloured shapes represent inputs to the system and white-coloured shapes are outputs.

Regarding the phytoplankton budget, sedimentation is the most important process although it is much lower than in X_{TSS} balance (Figure 10). The contribution of the growth process is very low.

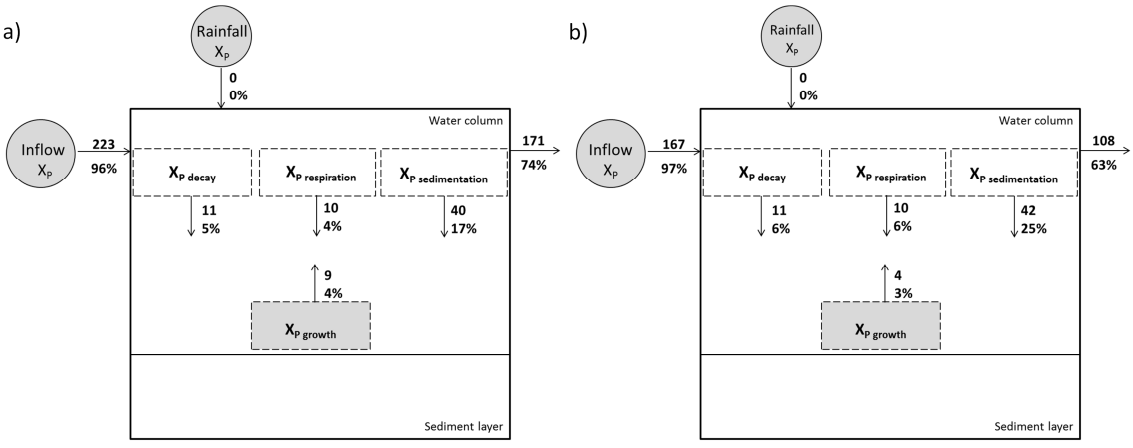

Figure 10. Phytoplankton budget (kg) for (a) FG1 and (b) FG2 as calculated from the model for April 2009-2012. Grey-coloured shapes represent inputs to the system and white-coloured shapes are outputs.

Sedimentation of the different particulate components including phytoplankton is the most important process in TP budget, with OP sedimentation being the most important one. Diffusion from sediment and resuspension processes have little influence in TP budget (Figure 11). The different influence of resuspension in TP and X_{TSS} budgets is a consequence of the low average phosphorus content measured in sediment (i_{Psed}=0.143 mg P g dw^{-1}) when compared to the range between 0.147-4.088 mg g^{-1} cited in bibliography (Kadlec and Wallace, 2009).

The amount of X_{TSS} and TP associated to rainfall can be considered negligible, as they represent less than 1% of the total inputs to the systems.

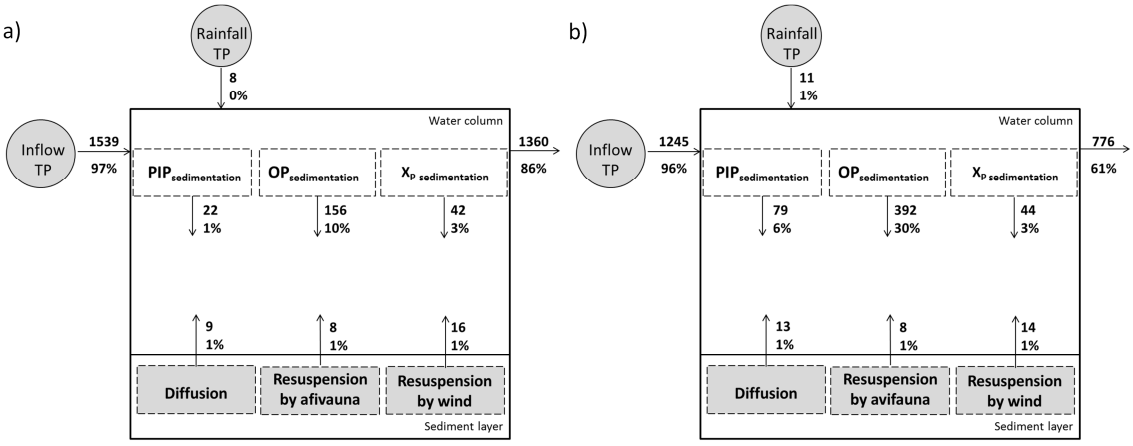

Figure 11. Total phosphorus budget (kg) for (a) FG1 and (b) FG2 as calculated from the model for April 2009-2012. Grey-coloured shapes represent inputs to the system and white-coloured shapes are outputs.

4. Conclusions

In this paper a new model has been described to simulate the concentrations of TSS, linked to phytoplankton and TP in free water surface CWs. In order to achieve this aim, the main processes involved have been modelled by developing kinetic equations. The software AQUASIM has been used to implement these model equations together with water flow. The model has been calibrated and validated comparing simulated and

observed outlet concentrations obtained in two full-scale FWSCWs named as FG1 and FG2, from April 2009 to April 2012. A sensitivity analysis has been carried out in order to clarify which are the most influential parameters.

The results reveal that the model suitably represents the concentrations of TSS, phytoplankton and TP. An outstanding innovation of this model is the link between phytoplankton and TSS, enabling researchers to quantify the contribution of phytoplankton to the TSS performance. Furthermore, the model distinguishes resuspension into that produced by wind and by avifauna activity respectively, and demonstrates that these are crucial processes to be included when modelling these components.

One of the most remarkable contributions of this paper is to model the effect of emergent vegetation cover in TSS, phytoplankton and TP performances and proves its crucial role in improving TSS sedimentation and preventing resuspension.

This model fills an existing gap in the development of mechanistic models in FWSCWs and enhances the knowledge about the processes that take place. Besides being able to implement future scenarios, the model is a useful support tool for designing and making decisions.

Acknowledgements

We would like to strongly thank to Pablo Vera (SEO/BirdLife) for him collaboration with waterfowl monitoring and data analysis and to Maria Antonia Rodrigo and Matilde Segura (ICBiBE, Universitat de València) for collecting Chl *a* data. We would also like acknowledge the support of Confederación Hidrográfica de Júcar (CHJ, MMARM) and the staff members in Tancat de la Pipa.

Appendix A

Parameter	Description	Units
a_{Xp}	Specific light attenuation coefficient of phytoplankton .	L mg^{-1} m^{-1}
$C_{et,n}$	Concentration in the evapotranspiration of the component *n.*	mg L^{-1}
$C_{gr,n}$	Concentration in the percolation flow of the component *n*.	mg L^{-1}
$C_{in,n}$	Inlet concentration of the component *n.*	mg L^{-1}
C_n	Outlet concentration of the component *n.*	mg L^{-1}
$C_{rf,n}$	Concentration in the rainfall of the component *n.*	mg L^{-1}
D_{0P}	Diffusion coefficient of DIP.	m^2 d^{-1}
DIP	Dissolved inorganic phosphorus.	
DO	Dissolved oxygen.	mg O_2 L^{-1}
dw	Dry weight.	
F	Fetch.	m
f	Photoperiod, the fraction of daylight.	
f_d	Dissolved fraction of the inorganic phosphorus.	
f_{POP}	Fraction of particulate organic phosphorus.	
F_{op}	Fraction of P recycled to OP in X_P decay.	
F_{pr}	Fraction of resuspended P recycled to OP.	
G_L	Light limitation in phytoplankton growth kinetics.	
G_{max}	Maximum growth rate for X_P at 20 ºC.	d^{-1}
H	Water depth.	m
I_0	Average incident daylight intensity.	ly d^{-1}
i_{Psed}	P content in the sediments.	mg P mg d.w.$^{-1}$

i_{PXp}	P content in phytoplankton tissues.	mg P mg $Chla^{-1}$
i_{TSSXp}	TSS content ratio in X_P.	mg dw mg $Chla^{-1}$
I_s	Saturating light intensity for X_P.	ly d^{-1}
K_{20}	Process rate at 20ºC.	d^{-1}
K_{avi}	Coefficient of resuspension by avifauna.	mg m^2 L^{-1} d^{-1}
K_d	Partition coefficient for inorganic phosphorus.	L mg^{-1}
$K_{difu\ sed}$	Coefficient of variation in the diffusion between water and sediments.	
k_{DIPup}	Saturation coefficient for DIP in P uptake by X_P.	mg P L^{-1}
k_{DO}	Saturation coefficient for DO in OP mineralization.	mg O_2 L^{-1}
$k_{DO\ Xp}$	Saturation coefficient for DO in X_P respiration.	mg O_2 L^{-1}
K_e	Extinction coefficient.	m^{-1}
K_{e0}	Light attenuation coefficient of water.	m^{-1}
$K_{min\ OP}$	OP mineralization rate at 20ºC.	d^{-1}
K_r	X_P decay rate at 20 ºC.	d^{-1}
K_{resp}	X_P respiration rate at 20 ºC.	d^{-1}
K_T	Process rate at temperature T.	d^{-1}
$K_{veg\ resus}$	Coefficient for trapping by emergent VC in resuspension processes.	
$K_{veg\ sed}$	Coefficient for trapping by emergent VC in sedimentation processes.	
L	Wavelength.	m
NSE	Nash-Sutcliffe efficiency.	

OP_{res}	OP entering to the system by wind resuspension.	mg P L^{-1}
PIP	Particulate inorganic phosphorus.	
PIP_{res}	PIP entering to the system by wind resuspension.	mg P L^{-1}
P_{max}	Maximum P_{int} rate for $X_{P.}$	mg P mg $Chla^{-1}$
$P_{max\ uptake}$	Maximum phosphorus uptake rate.	mg P mg $Chla^{-1}$ d^{-1}
P_{min}	Minimum P_{int} rate for X_P.	mg P mg $Chla^{-1}$
P_{sed}	Phosphorus concentration in interstitial water in sediments.	
Q_{et}	Evapotranspiration flow.	L s^{-1}
Q_{gr}	Gains/losses of the system by percolation to groundwater.	L s^{-1}
Q_{in}	Inlet flow.	L s^{-1}
Q_{out}	Outlet flow.	L s^{-1}
Q_{rf}	Direct rainfall flow entering to the system.	L s^{-1}
RF_i	Resuspension factor of the group of birds *i*.	
RMSE	Root mean square error.	
r_j	Reaction rate for process *j*.	d^{-1}
r_n	Reaction rate for the component *n*.	d^{-1}
t	Time.	s
T	Temperature.	ºC
TCOD	Total chemical oxygen demand.	mg O_2 L^{-1}
TSS	Total suspended solids.	
$X_{TSS\ res}$	TSS entering to the system by wind resuspension.	mg L^{-1}
V	Water volume.	L

VC	Vegetation cover, the fraction of the CW surface covered by vegetation.	
v_{sOP}	Sedimentation velocity of OP.	m d^{-1}
v_{sTIP}	Sedimentation velocity of TIP.	m d^{-1}
v_{sTSS}	Sedimentation velocity of TSS.	m d^{-1}
v_{sXp}	Sedimentation velocity of X_p.	m d^{-1}
W	Maximum daily wind speed.	m s^{-1}
W_0	Minimum wind speed to cause resuspension.	m s^{-1}
α	First coefficient of resuspension by wind.	
β	Second coefficient of resuspension by wind.	
θ	Temperature coefficient.	
θ_{difu}	Temperature coefficient for DIP diffusion.	
θ_G	Temperature coefficient for X_P growth.	
$\theta_{min\ OP}$	Temperature coefficient for mineralization of OP.	
θ_r	Temperature coefficient for X_P decay.	
θ_{resp}	Temperature coefficient for X_P respiration.	
$\upsilon_{n,j}$	Stoichiometric factor for component *n* and process *j*.	
δ(W,W0)	Step function that determines the periods when the wind-induced waves cause resuspension.	

598

599

600 **Bibliography**

601- Ambrose, Jr., R.B., Martin, J. L. and Wool, T.A., 1988. WASP4, A Hydrodynamic and
602 Water Quality Model -- Model Theory, User's Manual and Programmer's Guide.
603 USEPA, Athens, GA.

APHA, 1991. Standard Methods for the Examination of Water and Wastewater, 17th ed. American Publish Health Association, Washington, DC, USA.

Ballatore, T.J., Muhandiki, V.S., 2002. The case for a World Lake Vision. Hydrol. Process. 16, 2079–2089.

Baretta-Bekker, J.G., Baretta, J.W., Ebenhoh, W., 1997. Microbial Dynamics in the Marine Ecosystem Model {ERSEM} {II} with Decoupled Carbon Assimilation and Nutrient Uptake. Journal of Sea Research 38(3-4):195–211.

Calero, S., Segura, M., Rojo, C., Rodrigo, M.A., 2015. Shifts in plankton assemblages promoted by free water surface constructed wetlands and their implications in eutrophication remediation. Ecol. Eng., 74, 385–393.

Chapra, St. C., 1997. Surface Water-Quality Modeling. McGraw-Hill.

Chavan, P.V., Dennett, K.E., 2008. Wetland simulation model for nitrogen, phosphorus, and sediments retention in constructed wetlands. Water Air Soil Pollut. 187, 109-118.

Comín, F. A., Herrera-Silveira, J. A., Martín M., 1997. Flamingo footsteps enhance nutrient release from the sediment to the water column. Wetlands International Publication. 43:211-227.

Coveney, M.F., Stites, D.L., Lowe, E.F., Battoe, L.E., Conrow, R., 2002. Nutrient removal from eutrophic lake water by wetland filtration. Ecol. Eng. 19, 141–159.

Cózar A., Galvez, J.A., Hull V., García, C.M., Loiselle, S.A., 2005. Sediment resuspension by wind in a shallow lake of Esteros del Ibera (Argentina): a model based on turbidimetry. Ecol Model, 186: 63–76.

Di Toro D.M., O'Connor D.J., Thomann R.V., 1971. A dynamic model of the phytoplankton population in the Sacramento-San Joaquin delta. Adv. Chem. Ser., 106, 131-180 (1971).

628 Douglas, R.W., Rippey, B., 2000. The random redistribution of sediment by wind in a
629 lake. Limnol. Oceanogr. 45 (3), 686–694.
630 Giraldi, D., de Michieli Vitturi, M., Iannelli, R., 2010. FITOVERT: A dynamic
631 numerical model of subsurface vertical flow constructed wetlands. Environ. Modell.
632 Softw. 25, 633-640.
633 Glassom, D., Branch G.M., 1997. Impact of predation by greater flamingos
634 *Phoenicopterus ruber* on the macrofauna of two southern African lagoons, Mar. Ecol.
635 Prog. Ser. 150, 1–12.
636 Greenway, M., 2010. Wetlands and ponds for stormwater treatment in subtropical
637 Australia: their effectiveness in enhancing biodiversity and improving water quality? J.
638 Contemp. Water. Res. Edu. 146, 22-38.
639 Harter, S.K., Mitsch, W.J., 2003. Patterns of short-term sedimentation in a freshwater
640 created marsh. J. Environ. Qual. 32, 325–334.
641 Henze, M., Gujer, W., Mino, T., van Loosdrecht, M.C.M., 2000. Activated sludge
642 models ASM1, ASM2, ASM2D and ASM3. IWA Scientific and Technical Report No.9,
643 IWA Publishing, London, UK.
644 Hosokawa Y., Horie T., 1992. Flow and particulate nutrient removal by wetland with
645 emergent macrophyte. Sci. Total Environ. 1271–1282.
646 ISO 11263:1994. Soil quality. Determination of phosphorus. Spectrometric
647 determination of phosphorus soluble in sodium hydrogen carbonate solution.
648 Jeffrey, S.W., Humphrey, G.P., 1975. New spectrophotometric equations for
649 determining chlorophylls a, b, c1 and c2 in higher plants, algae and natural
650 phytoplankton. Biochem. Physiol. Pflanzen. 19, 191–194.
651 Kadlec, R.H., Knight, R.L., 1996. Treatment Wetlands. CRC Press, Boca Raton, FL 893
652 pp.

653 Kadlec, R.H., 1997. An autobiotic wetland phosphorus model. Ecol. Eng., 8(2), 145–
654 172.
655 Kadlec, R.H., Wallace, S.D., 2009. Treatment Wetlands, Second Ed. CRC Press, Boca
656 Raton, FL.
657 Langergraber, G., 2001. Development of a simulation tool for subsurface flow
658 constructed wetlands. Ph.D. thesis. Wiener Mitteilungen 169, Vienna, Austria.
659 Langergraber, G., Rousseau, D., García, J., Mena, J., 2009. CWM1 - A general model to
660 describe biokinetic processes in subsurface flow constructed wetlands. Water Sci.
661 Technol. 59, 1687-1697.
662 Langergraber, G., Šimůnek, J., 2012. Reactive Transport Modeling of Subsurface Flow
663 Constructed Wetlands Using the HYDRUS Wetland Module. Vadose Zone Journal,
664 11(2).
665 Martín, M., 1998. Modelación de la Calidad en Aguas Superficiales. Aplicación al caso
666 de la Albufera de Valencia. Ph.D. thesis. University of Valencia. Spain.
667 Martín, M., Oliver, N., Hernández-Crespo, C., Gargallo, S.,Regidor, M.C., 2013. The
668 use of free water surface constructed wetland to treat the eutrophicated waters of lake
669 L'Albufera de Valencia (Spain). Ecol. Eng. 50, 52–61.
670 Mburu, N., Sanchez-Ramos, D., Rousseau, D.P.L., van Bruggen, J.J.A., Thumbi, G.,
671 Stein, O.R., Hook, P.B., Lens, P.N.L., 2012. Simulation of carbon, nitrogen and sulphur
672 conversion in batch-operated experimental wetland mesocosms. Ecol. Eng. 42, 304–
673 315.
674 Meyer, D., Chazarenc, F., Claveau-Mallet, D., Dittmer, U., Forquet, N., Molle, P.,
675 Morvannou, A., Pálfy, T., Petitjean, A., Rizzo, A., Samsó, R., Scholz, M., Soric, A.,
676 Langergraber, G., 2015. Modelling constructed wetlands: Scopes and aims – a
677 comparative review. Ecol. Eng. 80, 205-213.

Min, J.H., Paudel, R., Jawitz, J.W., 2011. Mechanistic biogeochemical model applications for Everglades restoration: a review of case studies and suggestions for future modeling needs. Critic. Rev. Environ. Sci. Technol. 41, 489-516.

Mulling, B.T.M., 2013. Particles matter: Transformation of suspended particles in constructed wetlands.

Nagid, E.J., Canfield, D.E., Hoyer, M.V., 2001. Wind-induced increases in trophic state characteristics of a large (27 km2), shallow (1.5 mean depth) Florida lake. Hydrobiologia 455, 97–110.

Onandia, G., Gudimov, A., Miracle, M. R., Arhonditsis, G., 2015 Towards the development of a biogeochemical model for addressing the eutrophication problems in the shallow hypertrophic lagoon of Albufera de Valencia, Spain. Ecol. Inform. 26, 70–89.

Paudel, R., Jawitz, J.W., 2012. Does increased model complexity improve description of phosphorus dynamics in a large treatment wetland? Ecol. Eng. 42, 283-294.

Reddy, K.R., DeLaune, R.D., 2008. Biogeochemistry of wetlands: science and applications. CRC press.

Reichert, P. 1998. AQUASIM 2.0 - User Manual Computer Program for the Identification and Simulation of Aquatic Systems. Swiss Federal Institute for Environmental Science and Technology (EAWAG), CH-8600 Dubendorf, Switzerland.

Reynolds, C.S., 2006. The Ecology of Phytoplankton. Cambridge, UK. Cambridge University Press.

Reichert, P., Borchardt, D., Henze, M., Rauch, W., Shanahan, P., Somlyódy, L., Vanrolleghem, P., 2001. River Water Quality Model No.1. IWA Publishing.

Rivers-Moore, N.A., de Moor, F.C., Birkholz, S.A., Palmer, R.A., 2006. Estimation of preferred water flow parameters for four species of *Simulium* (Diptera: Simuliidae) in small clear streams in South Africa. Afr. J. Aquat. Sci. 31, 261–269.

Samsó, R., García, J., 2013. BIO_PORE, a mathematical model to simulate biofilm growth and water quality improvement in porous media: application and calibration for constructed wetlands. Ecol. Eng. 54, 116–127.

Scheffer, M., Hosper, S. H., Meijer, M. L., Moss, B., Jeppesen, E., 1993. Alternative equilibria in shallow lakes. Trends Ecol. Evol. 8, 275-279.

Schmid, B.H., Stephan, S., Hengl, M.A., 2005. Sediment deposition in constructed wetland ponds with emergent vegetation: laboratory study and mathematical model. Wat. Sci. Tech. 51 (9), 307–314.

Schmidt, C., Musolff, A., Trauth, N., Vieweg, M., Fleckenstein, F.H., 2012. Transient analysis of fluctuations of electrical conductivity as tracer in the stream bed. Hydrol. Earth Syst. Sci. 16, 3689–3697.

Søndergaard, M., Kristensen, P., Jeppesen, E., 1992. Phosphorus release from resuspended sediment in the shallow and windexposed Lake Arresø, Denmark. Hydrobiologia 228: 91–99.

Stone, K.C., Poach, M.E., Hunt, P.G., Reddy, G.B., 2004. Marsh-pond-marsh constructed wetland design analysis for swine lagoon waste water treatment. Ecol. Eng. 23, 127-133.

Tsanis, I. K., Prescott, K. L., Shen, H., 1998. Modelling of Phosphorus and Suspended Solids in Cootes Paradise Marsh. Ecol. Model. 114(1):1–17.

UNEP, 1994. The Pollution of Lakes and Reservoirs. Environ Libr., 10, 1–36.

Wang, N., Mitsch, W.J., 2000. A detailed ecosystem model of phosphorus dynamics in created riparian wetlands. Ecol. Model. 126, 101–130.

Wang, N., Mitsch, W. J., 2000. A detailed ecosystem model of phosphorus dynamics in created riparian wetlands. Ecol. Model., 126(2-3), 101–130.

Wang, Y. C., Lin, Y. P., Huang, C. W., Chiang, L. C., Chu, H. J., Ou, W. S., 2012. A system dynamic model and sensitivity analysis for simulating domestic pollution removal in a freewater surface constructed wetland. Water Air Soil Pollut. 223(5), 2719–2742.

Weyhenmeyer, G.A., Hakanson, L., Meili, M., 1997. A validated model for daily variations in the flux, origin and distribution of settling particles within lakes. Limnol. Oceanogr. 42 (7), 1517–1529.

Wu, H., Huang, P., Wang, J., 2010. Treatment of eutrophic-lake water by free water surface wetland. World Academy of Science. Eng. Technol., 67.